JOURNAL OF SOLID STATE CHEMISTRY **141,** 282–289 (1998)
ARTICLE NO. SC988004

Preparation and Electrical Characterization of Ruthenia-Doped Yttria-Stabilized Zirconia Ceramics

M. T. Colomer[1] and J. R. Jurado

Instituto de Cerámica y Vidrio, CSIC, Antigua Ctra. Valencia Km. 24,300, 28500 Arganda del Rey, Madrid, Spain

Received December 30, 1997; in revised form August 3, 1998; accepted August 7, 1998

Samples belonging to the $[(ZrO_2)_{0.92}(Y_2O_3)_{0.08}]_{1-x}(RuO_2)_x$ system, where $0 \leq x \leq 0.1$ (mol), have been synthesized by a polymeric sol–gel route and sintered in air at 1400°C for 2 h. The RuO_2–YSZ solid solution limit is found at $x = 0.05$ at 1400°C by X-ray diffraction and electrochemical impedance spectroscopy measurements. The electrical conductivity of the studied materials decreases with ruthenia additions. At high temperature (700–850°C) and low oxygen partial pressure, these materials behave as mixed oxygen ion–electronic conductors. The electronic conductivity as a function of P_{O_2} shows a dependence of $-1/4$ and an activation energy of 0.98 eV. The electronic contribution is explained on the basis of redox equilibrium between trivalent Ru^{3+} and divalent Ru^{2+}. The EPR spectra of polycrystalline sintered samples confirm the presence of Ru^{3+}. © 1998 Academic Press

INTRODUCTION

Ruthenium oxide, RuO_2, is a transition metal dioxide and has been known for several years to be a very active catalyst in anodic processes such as Cl_2 or O_2 evolution and cathodic reduction of O_2 (1–6). In addition, the capability of RuO_2 to adsorb hydrogen reversibly may play an important role for CO_2 reduction (7). Finally, RuO_2 is used as a catalyst in the Fischer–Tropsch conversion of carbon monoxide to either hydrocarbons or alcohols (8). However, RuO_2 undergoes a strong volatilization process above 800°C in air (9), which makes it difficult to use this oxide or related materials at higher temperatures. In addition, RuO_2 suffers a reduction to metallic Ru under reducing conditions (10). To increase the chemical and thermal stability of this oxide, it is necessary to use a matrix which accommodates and stabilizes it. If the stability were increased, it would allow higher operation temperatures in the above-described processes and enhanced efficiency. However, catalytic studies are also needed to assess if the activity of RuO_2 is retained.

[1] To whom correspondence should be addressed. E-mail: tcolomer@icv.csic.es.

Long *et al.* (10) prepared solid solutions of Ru(IV)/ZrO_2 and $RuO_2/(La_2O_3/ZrO_2)$ by decomposing the required mixture of ruthenium nitrosyl nitrate $[Ru(NO)(NO_3)_3]$ and zirconyl nitrate $[ZrO(NO_3)_2]$, and ruthenium nitrosyl nitrate, lanthanum nitrate, and zirconyl nitrate, respectively. They concluded that a solid solution of Ru(IV) oxide in ZrO_2 increases the temperature of reduction of ruthenium oxide in hydrogen from under 90°C to over 200°C. The further addition of 5 mol% of lanthanum (III) oxide significantly increases the reduction temperature of dispersed RuO_2, allowing its use at temperatures as high as 800°C.

Hammou *et al.* (11) and Djurado *et al.* (12) prepared ternary oxide samples of ZrO_2, Y_2O_3, and RuO_2 by the Long method (10) to give nominal compositions $[(ZrO_2)_{0.91}(Y_2O_3)_{0.09}]_{1-x}(RuO_2)_x$ ($0 \leq x \leq 0.2$ mol of RuO_2). They reported cubic zirconia solid solutions with $0 \leq x < 0.125$ mol of RuO_2 sintered at 900°C in air.

Recently, Colomer and Jurado (13) have obtained by a polymeric sol–gel route ruthenia-doped yttria-stabilized zirconia solid solutions stable in air at temperatures as high as 1400°C.

Spears and Tuller (14,15) studied the mixed ionic and electronic conductivity in ruthenium-substituted gadolinium titanate $Gd_2(Ru_xTi_{1-x})_2O_{7-\delta}$. They reported the electrical conductivity behavior and outlined a defect chemical model that incorporates the multiple valences of ruthenium ion.

On the other hand, yttria-stabilized zirconia (YSZ) based materials with mixed valence dopants (e.g., Ce or Ti) are known to exhibit broad mixed conduction domains, depending on dopant nature, concentration, and temperature. Although ceria- and titania-doped materials have been studied for a number of years (16–37), ruthenia-doped yttria-stabilized zirconia materials have not yet been studied from this point of view.

In this paper, gels with nominal $[(ZrO_2)_{0.92}(Y_2O_3)_{0.08}]_{1-x}(RuO_2)_x$ compositions, where $x = 0$, 0.05, 0.08, and 0.1 (mol), were synthesized by the polymeric sol–gel technique. After sintering in air at 1400°C, structural and electrochemical characterization of the ceramic

0022-4596/98 $25.00

compacts obtained was carried out in air and under reducing conditions.

EXPERIMENTAL

Samples studied in this work were prepared by a polymeric sol–gel process as described elsewhere (13). Compositions with $[(ZrO_2)_{0.92}(Y_2O_3)_{0.08}]_{1-x}(RuO_2)_x$, where $x = 0$, 0.05, 0.08, and 0.1 mol, were synthesized. The conventional solid-state reaction was also tested to obtain ceramic materials with the described composition. Despite the use of a $RuO_3 + RuO_4$ rich atmosphere (buffer) and fast firing method (heating and cooling rate of $20^\circ C\,min^{-1}$), the samples obtained after sintering at temperatures between 900 and 1400°C exhibited high porosity and contained no Ru due to the complete volatilization of RuO_2. Gels were prepared from analytical grade ruthenium (III) acetylacetonate (acac) (Merck, zirconium (IV) *n*-propoxide (Fluka), and 99.9% pure hydrated yttrium acetate (Aldrich). They were dried slowly by covering them with a plastic film to slow solvent loss by evaporation. Holes were made in the film with a needle to control the rate of evaporation (38). Monolithic, scarlet-colored, translucent gels were obtained, except for the YSZ sample. In the latter case, the dry gel was transparent and colorless. The gels were thermally treated at several temperatures between 200 and 700°C with 12 h of soaking time. Sintering was carried out in air at 1400°C for 2 h, at a heating and cooling rate of $5^\circ C\,min^{-1}$.

Differential thermal and thermogravimetric analyses (DTA–TGA) were carried out in a Perkin-Elmer thermoanalyzer under air using a platinum crucible and a heating rate of $20^\circ C\,min^{-1}$. Finely powdered alumina was used as a reference substance. Evolution of crystalline phases was followed by XRD (Siemens D-5000 diffractometer) using Cu$K\alpha_1$ radiation and a Ni filter. To determine the porosity in the sintered samples a Micromeritics Autopore II 9220 Hg porosimeter was used, with an intrusion pressure range between 1.33 and 414 MPa and a resolution power of $\pm 1\%$ of full scale, that is, 0.207 MPa. A penetrometer of 6.12-cm^3 volume and a pressure of 1 torr were used in which previously degasified samples were studied at room temperature. A cycle with 200 experimental points over the whole pressure range was chosen. EPR spectra were measured at 77 and 300 K. The magnetic cavity of the spectrometer (Bruker Model Esp 300E) was tuned to 100 kHz of modulation frequency and the magnetic field was scanned from 400 to 4000 G. Irradiated quartz was used as a reference for $g = 2.003$. The modulation amplitude was 5 G, the conversion time 81.92 ms, the time constant 20.48 ms, and the X-band microwave frequency 9.75 GHz. Impedance spectroscopy measurements (EIS) were performed in air between 250 and 900°C in the 5- to 10^7-Hz frequency range (HP 4192A impedance analyzer), and electrical conductivity measurements as a function of oxygen partial pressure were performed in a controlled-atmosphere furnace using a YSZ sensor and a YSZ electrochemical pump (39, 40).

In the following, ruthenia-doped yttria-stabilized zirconia will be labeled 100RuYSZ.

RESULTS AND DISCUSSION

DTA and TGA

All the DTA and TGA curves exhibit similar characteristics for the different compositions studied. Figure 1 shows the 10RuYSZ dried gel DTA–TGA curve. In the temperature range 50–160°C, the endothermic peak observed is associated with (a) the evaporation of the residual absolute ethanol used as organic solvent in the synthesis, (b) the evaporation of the acetic acid used in the synthesis, (c) the *n*-propanol formed during the hydrolysis of the zirconium (IV) *n*-propoxide, and (d) the evaporation of the water formed during the polycondensation. This is confirmed by the weight loss (12%) detected in this temperature interval in the TGA curve.

An inflection is observed at 260°C in the DTA curve and is attributed to the loss of the absolute ethanol, *n*-propanol, and water trapped in the pores of the gel. This fact is associated with a weight loss that is observed in the TGA curve. The exothermic peak detected between 210 and 320°C is associated with the combustion of the organic material. The TGA curve shows a strong weight loss (21%), indicating that there is a noncrystallization process, which agreed well with the exothermic peak observed. The RuO_2 and RuYSZ solid solution crystalline phases were detected in the residual ash. In the temperature range 1325–1400°C, a slight weight loss was detected, which is likely due to a partial volatilization of RuO_2 that does not enter in solid solution into the fluorite lattice (10RuYSZ sample).

For $x = 0$, 0.05, and 0.08 no weight loss was observed in that temperature range.

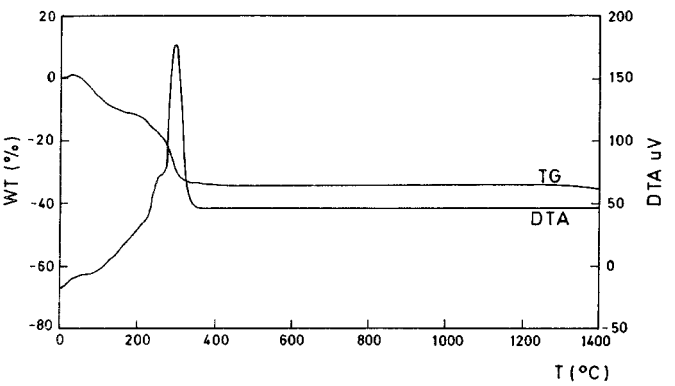

FIG. 1. DTA–TGA curves of the dry gel of composition 10RuYSZ.

XRD

The XRD patterns of the dried gels indicated that an amorphous structure was achieved. For the calcined gel with $x = 0.05$, at temperatures as low as 500°C, a cubic zirconia single phase was obtained (Fig. 2), indicating the very high reactivity of the powders obtained, as is expected with the processing method used. According to the literature (41), low organic retention (slow drying) allows a higher crystalline phase development, as is observed in this work.

At 500°C for the sample with $x = 0.08$, the cubic zirconia single phase is also maintained. For the sample with $x = 0.1$, the peaks of RuO_2 confirm the ruthenium segregation (Fig. 3).

Djurado *et al.* (12) indicated that samples should be fired up to 900°C to avoid thermal decomposition. They studied the chemical stability of the new oxides with temperature; then samples were sintered at 1400°C. The X-ray profiles of these samples were the same as those of pure YSZ, implying a total RuO_2 volatilization in their samples at this sintering temperature. In this work and at that temperature (1400°C), the unit cell parameter changed from 0.5137(2) nm for pure YSZ to 0.5104(3) nm for 5RuYSZ; these results demonstrate that the sol–gel technique is suitable to obtain ruthenia-doped YSZ materials at temperatures as high as 1400°C. A similar value was achieved for 8RuYSZ, 0.5103 (3) nm, indicating that part of the RuO_2 is segregated. This fact is confirmed in the sample 10RuYSZ, where the peaks of RuO_2 are clearly observed (Fig. 4).

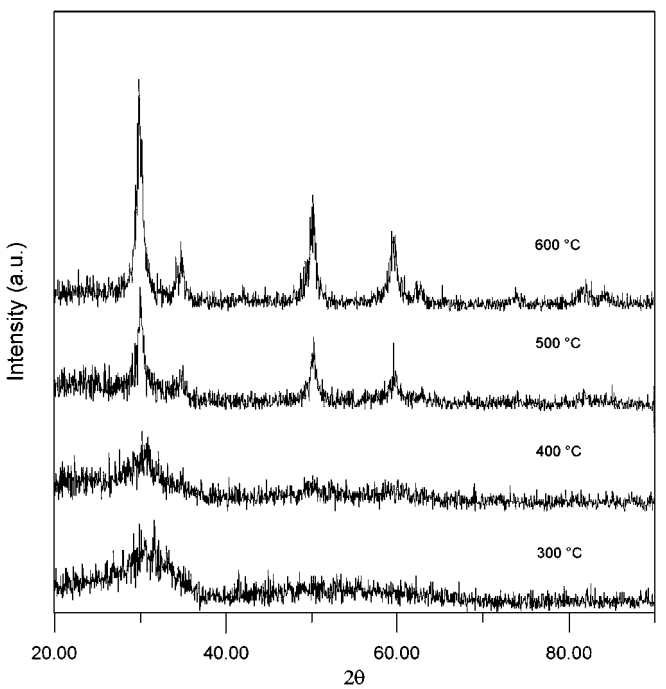

FIG. 2. X-ray powder diffraction patterns of calcined gel with $x = 0.05$ at different temperatures.

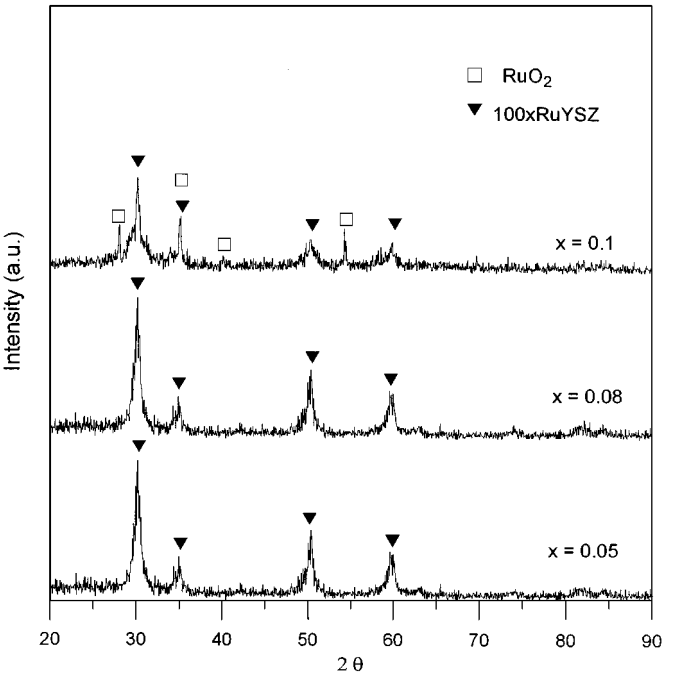

FIG. 3. X-ray diffraction spectra of samples with $x = 0.05$, 0.08, and 0.1 at 500°C.

EPR Measurements

To confirm the existence of Ru^{3+} in the sintered samples, EPR studies were conducted. The EPR spectrum (Fig. 5b) of the opaque, polycrystalline 10RuYSZ shows absorption peaks at $g = 4.16 \pm 0.01$ and $g = 2.22 \pm 0.01$. The former peak is attributed to the high-spin ($\pm$ 5/2) transition of iron impurities in the 3+ oxidation state (< 0.04 wt%), and it is in agreement with EPR measurements in yttria (12 mol%)-stabilized zirconia–titania having 1–15 mol% TiO_2 reported by Swider and Worrell (42). Concerning the second peak, the ruthenium paramagnetic ions are Ru^{+} ($4d^7$), Ru^{3+} ($4d^5$), and Ru^{5+} ($4d^3$), which are normally found in a low-spin configuration. Ru^{+} in oxidation conditions is not stable. The presence of a peak at $g = 2.22 \pm 0.01$ can be ascribed to Ru^{3+} and/or Ru^{5+}, but according to Sass *et al.* (43), only Ru^{5+} can appear in extreme oxidation conditions at temperatures as low as 325°C. The Ru^{5+} signal disappears when the temperature increases. It is, thus, believed that the small signal at $g = 2.22 \pm 0.01$ can be assigned to Ru^{3+}. This type of ion can thus be stabilized in the coordination sphere of Zr^{4+} (43).

For comparison, the EPR spectrum of a pure YSZ sample is shown in Fig. 5a, where only one peak is observed, corresponding to the high-spin ($\pm$5/2) transition of iron impurities in the 3+ oxidation state.

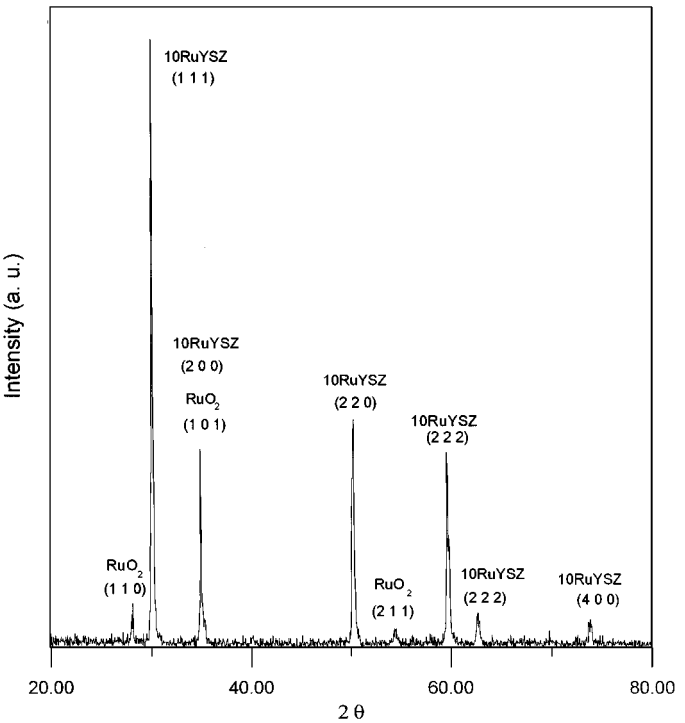

FIG. 4. XRD pattern of a 10RuYSZ sintered sample at 1400°C.

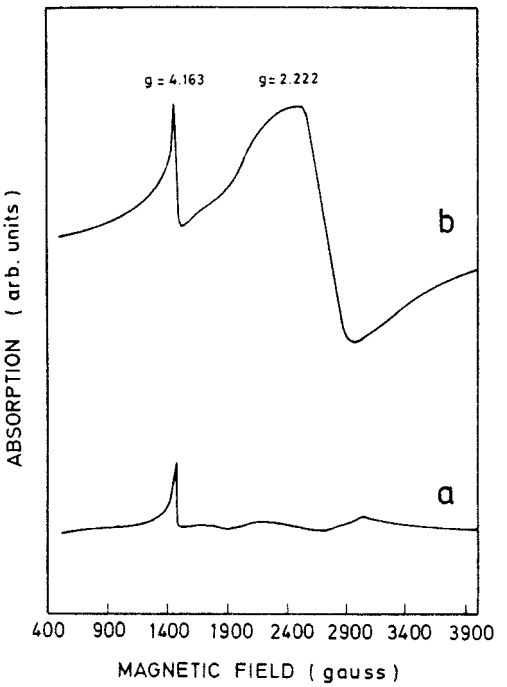

FIG. 5. (a)First-derivative EPR spectrum of 10RuYSZ at 300 K. (b) First-derivative EPR spectrum of YSZ at 300 K.

Impedance Spectroscopy in Air

Results obtained by impedance spectroscopy in air at 400°C for the compositions $[(ZrO_2)_{0.92}(Y_2O_3)_{0.08}]_{1-x}(RuO_2)_x$ where $x = 0$ and 0.05 (mol) are shown in Fig. 6 as representative examples. For 5RuYSZ, a small arc at high frequency was detected which could be attributed to the grain interior conductivity contribution (GI). A larger arc, situated in the low- and intermediate-frequency ranges, was also observed; this arc could be associated with the interface conductivity contributions (grain boundaries, electrode–electrolyte interface, and porosity). The compact ceramics obtained exhibited a porosity of about 10% for the sample 5RuYSZ, and the porosity increases with the RuO_2 concentration.

From the EIS spectra, the dependence of σ_{GI} vs $[RuO_2]$ at 400°C was obtained (Fig. 7) and this shows that in the range $0 < x \leq 0.05$ the lattice conductivity falls significantly (one and a half orders of magnitude). For the highest RuO_2 concentrations, σ_{GI} remains constant. The electrical activation energy determined was 1.10 eV for the bulk contribution (high-frequency small arcs) and 1.20 eV for the interfacial contribution (intermediate-frequency large arcs); these values are typical and characteristic of YSZ materials.

The ruthenia addition seems to be responsible for a decrease in oxygen mobility, which may be mainly explained by lattice distortion (decreasing lattice parameter), which is due to the replacement of the Zr^{4+} ions (radius Zr^{4+} (VIII) = 0.084 nm) by the smaller Ru^{4+} (VI) ions (radius Ru^{4+} (VI) = 0.062 nm) (44). The dependence of σ_{GI} vs $[RuO_2]$ could indicate that the solid solution limit of RuO_2 in YSZ would be located at $x = 0.05$, according to the XRD measurements.

An additional contribution to the decrease in ionic conductivity may be proposed by analogy with the behavior of YSZ containing TiO_2 . Traqueia and coauthors (45)

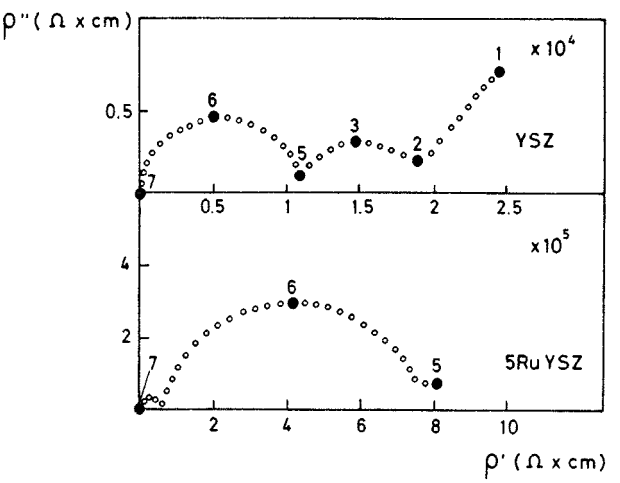

FIG. 6. Impedance spectroscopy arcs, in air at 400°C, for the compositions YSZ and 5RuYSZ.

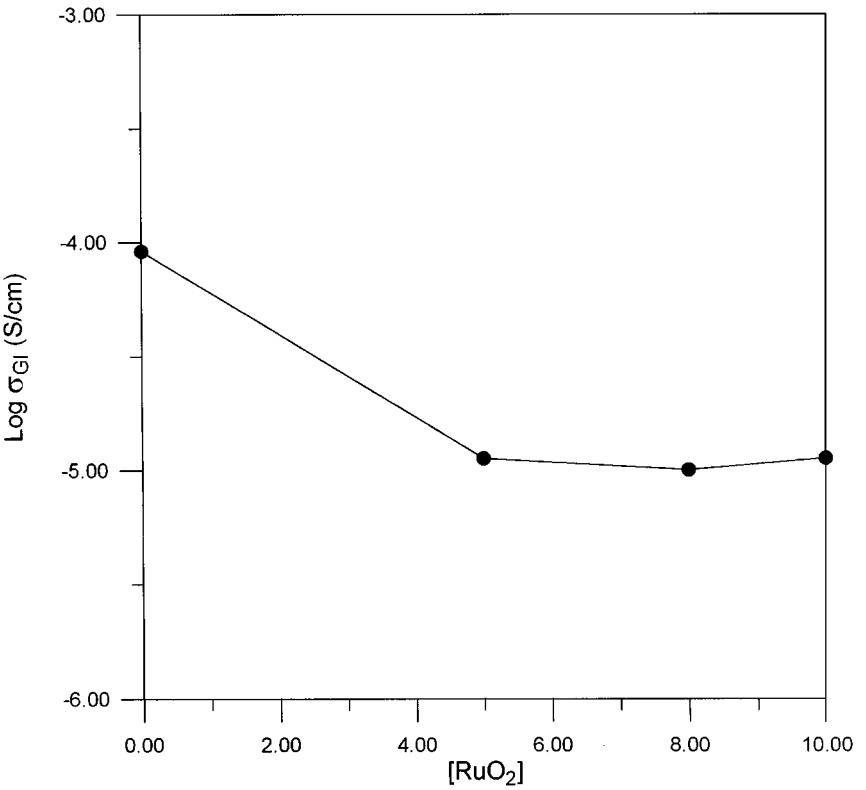

FIG. 7. Dependence of grain interior conductivity on RuO_2 concentration at 400°C in air.

suggested that the additive (TiO_2) may act as traps for the oxygen vacancies by shifting from the eightfold coordinated Zr site toward their preferred sixfold coordination; this was demonstrated by Raman spectroscopy studies for the Ti-containing materials. Note that TiO_2 and RuO_2 have the same rutile-type structure.

Dependence of Electrical Conductivity on P_{O_2}

Figure 8 shows log σ versus log P_{O_2} 10RuYSZ at 800°C. It must be noted that the fixed frequency used (10 kHz) is located in the interfacial arc. This fact implies that the studied material region is the electrode–electrolyte interface rather than the bulk region.

The σ versus P_{O_2} curves of the RuYSZ samples at different temperatures (700, 750, 800, and 850°C) exhibit identical dependencies on the oxygen partial pressure. Following a plateau at moderately oxidizing conditions, the conductivity increases with increasing reducing conditions, with a transition to a $-1/4$ slope on further reduction. This result is accord with the increase in electronic defects associated with the reduction of ruthenium ions:

$$O_o^x + 2Ru'_{Zr} \leftrightarrow \tfrac{1}{2}O_2 + V\ddot{o} + 2Ru''_{Zr}. \quad [1]$$

The Kroger–Vink type of notation for defects has been used in this reaction (46). In particular, the symbol Ru'_{Zr} corresponds to one electronic defect localized in a ruthenium ion in the cation sublattice (small polaron). In this manner, the electronic conductivity dependence on the oxygen partial pressure is expressed by the power $-1/4$. In fact, based on the expression for the equilibrium constant

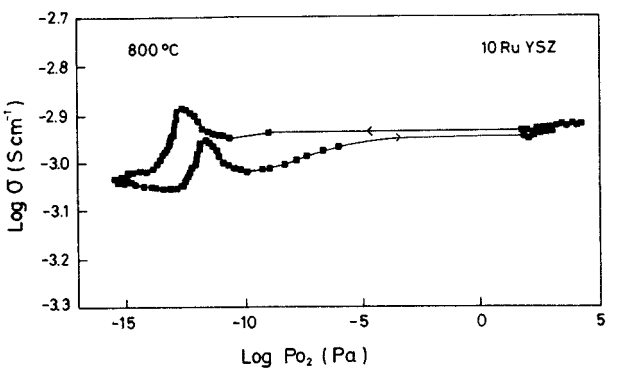

FIG. 8. Dependence of electrical conductivity (10 kHz) on oxygen partial pressure for 10RuYSZ at 800°C.

of reaction [1], K_1,

$$K_1 = P_{O_2}^{1/2}\,[V\ddot{o}]\,[Ru''_{Zr}]^2/[O_o^x]\,[Ru'_{Zr}]^2 \qquad [2]$$

This implies that

$$[Ru''_{Zr}] \propto P_{O_2}^{-1/4}. \qquad [3]$$

A maximum of conductivity (1.3×10^{-3} S/cm) is observed at 2.3×10^{-13} Pa (at 800°C) and shifts to lower P_{O_2} values as temperature decreases. Assuming hopping from Ru^{2+} to Ru^{3+}, one should expect an additional conductivity contribution and this should increase with the product of fractions $[Ru'_{Zr}][Ru''_{Zr}]$. This product is expected to attain a maximum value when $[Ru'_{Zr}] \approx [Ru''_{Zr}]$. One may also predict the effect of working conditions by examination of Eq. [1]. For example, on moving toward oxidizing conditions, one expects a limiting upper value for $[Ru'_{Zr}]$ and the concentration of Ru''_{Zr} must drop by about one order of magnitude when P_{O_2} drops by four orders of magnitude. The reverse is expected on moving toward very reducing conditions, when $[Ru''_{Zr}]$ reaches an upper value and $[Ru'_{Zr}]$ may drop by orders of magnitude.

For the lowest P_{O_2} investigated, the σ level is lower than the value found at the ionic plateau. This coincides with the behavior observed in Fig. 9. This figure shows the impedance spectra in air and at a $P_{O_2} = 1.76 \times 10^{-16}$ Pa (750°C) for 5RuYSZ and for 10RuYSZ (700°C), respectively. In these conditions, the total conductivity for all of the samples was higher in air that in reducing atmosphere, indicating a better electrical response of these materials in oxidizing conditions.

According to the model of defect chemistry, an n-type conductivity with a $-1/4$ slope is predicted under the reducing conditions. The hopping model predicts a local maximum in total conductivity at low P_{O_2} values, due to the hopping between the Ru^{3+} and Ru^{2+} states, such as noted in this work (Fig. 8). The activation energy obtained for this process is 0.98 eV. Similar results were reported by Spears and Tuller for ruthenium-substituted gadolinium titanate (14,15).

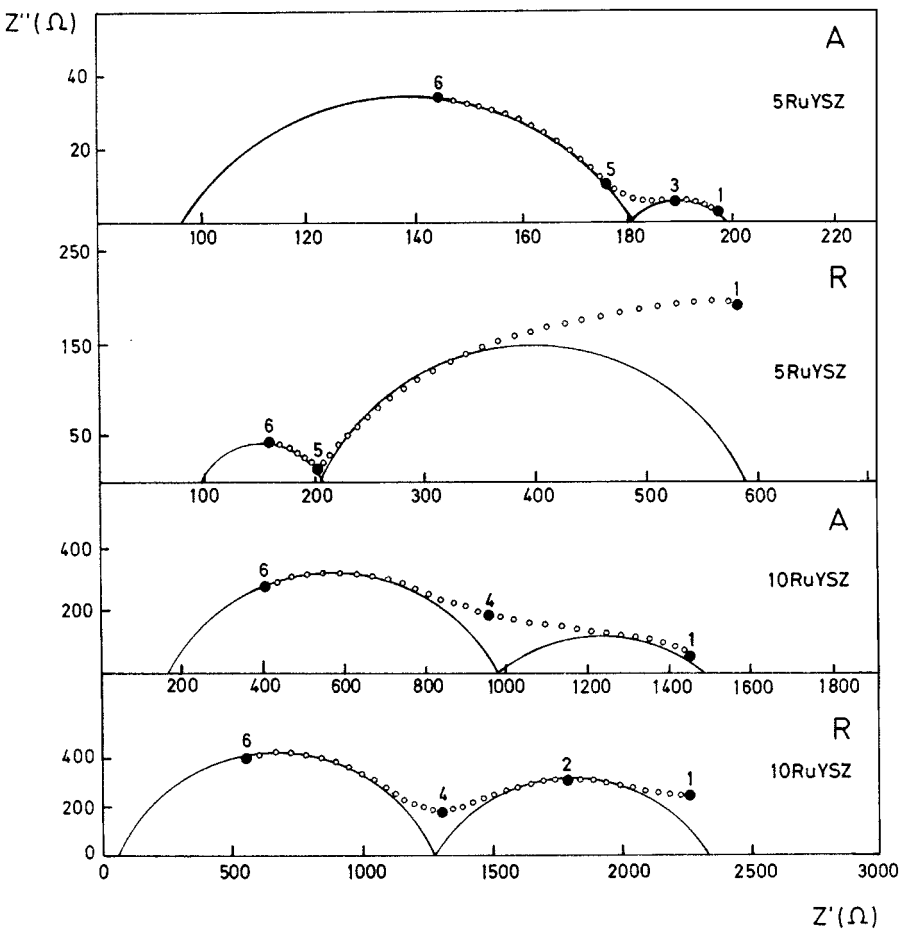

FIG. 9. Impedance plots in air of compositions 5RuYSZ (750°C) and 10RuYSZ (700°C) in air (A) and in reducing atmosphere (R).

A similar local maximum might be predicted under more oxidizing conditions, which is not observed experimentally due to hopping between the Ru^{4+} and Ru^{3+} states:

$$O_o^x + 2Ru_{Zr}^x \leftrightarrow \tfrac{1}{2}O_2 + V\ddot{o} + 2Ru'_{Zr}. \qquad [4]$$

In this manner, the electronic conductivity dependence on oxidizing conditions is expressed by the power 1/4. In fact, based on the expression for the equilibrium constant of reaction [4], K_2,

$$K_2 = P_{O_2}^{1/2}[V\ddot{o}][Ru'_{Zr}]^2/[O_o^x][Ru_{Zr}^x]^2. \qquad [5]$$

During the reoxidation process, the conductivity of the samples recover to the initial conditions.

The defect equilibrium reactions used to model RuYSZ are summarized in Table 1.

For $x = 0$, there is no maximum in the P_{O_2} range studied.

CONCLUSIONS

Ruthenia-doped yttria-stabilized zirconia solid solutions are obtained by a polymeric sol–gel synthesis and sintering in air at 1400°C. The solid solution limit at 1400°C in the $[(ZrO_2)_{0.92}(Y_2O_3)_{0.08}]_{1-x}(RuO_2)_x$ system is located at $x = 0.05$ by XRD and EIS measurements. The impedance spectra show a small arc, which is associated with the RuO_2–YSZ solid solution bulk (grain interior conductivity contribution). The decreasing bulk conductivity as RuO_2 is introduced seems to be due to a decrease in oxygen mobility, which may be mainly explained by lattice distortion. The total conductivity as a function of P_{O_2} shows a dependence of $-1/4$ and an activation energy of 0.98 eV, characteristic of electron hopping between ions. The electronic contribution is explained on the basis of redox equilibrium between trivalent Ru^{3+} and divalent Ru^{2+}. EPR studies confirm the existence of Ru^{3+} in the sintered samples.

TABLE 1
Defect Equilibrium Reactions in the ZrO_2–Y_2O_3–RuO_2 System

Reaction	Equilibrium
Intrinsic	
$O_o^x \leftrightarrow O_i'' + V\ddot{o}$	$K_{ri1} = [O_i''][V\ddot{o}]$
$e_v \leftrightarrow e' + h^{\cdot}$	$K_{ri2} = np$
Reduction	
$O_o^x \leftrightarrow \frac{1}{2}O_2\ (g) + V\ddot{o} + 2e'$	$K_r = P_{O_2}^{1/2}[V\ddot{o}]n^2$
Ruthenium ionization	
$Ru_{Zr}^x + e' \leftrightarrow Ru'_{Zr}$	$K_{ri3} = [Ru'_{Zr}]/[Ru_{Zr}^x]n$
$Ru'_{Zr} + e' \leftrightarrow Ru''_{Zr}$	$K_{ri4} = [Ru''_{Zr}]/[Ru'_{Zr}]n$
Charge Neutrality	
$n + 2[O_i''] + [F'_M] + [Ru'_{Zr}] + [Ru''_{Zr}] = p + 2\ [V\ddot{o}]$	

ACKNOWLEDGMENTS

The authors are grateful to Professors J. R. Frade and F. M. B. Marques from Aveiro University (Ceramic and Glass Department), the former for useful discussions and the latter for electrical conductivity versus P_{O_2} measurements carried out in his laboratory. Thanks are due to Professor J. Soares from Aveiro University (Physics Department) for the EPR measurements. This work has been supported by the Comission of the European Communities (Project JOUE-0044C).

REFERENCES

1. O. de Nora, *Chem.- Ing.- Techn.* **42,** 222 (1970).
2. A. T. Kuhn and C. S. Mortimer, *J. Electrochem. Soc.* **120,** 231 (1973).
3. S. Trassati and G. Lodi, *in* "Electrodes of Conductive Metallic Oxide" (S. Trassati, Ed.). Elsevier, Amsterdam/New York, 1981.
4. A. Bandi, I. Vartires, A. Mihelis, and C. Hainarosie, *J. Electroanal. Chem.* **157,** 241 (1983).
5. K. Ogura and M. Takagi, *Solar Energy* **37,** 41 (1986).
6. A. Bandi, A. Mihelis, I. Vartires, E. Ciortan, and I. Rosu, *J. Electrochem. Soc.* **134,** 1982 (1987).
7. T. Hepel, F. H. Pollak, and W. E. O'Grady, *J. Electrochem. Soc.* **131,** 2094 (1984).
8. S. R. Morris, R. B. Moyes, and P. B. Wells, *in* "Metal Support and Metal Additive Effects in Catalysis," (B. Imelik, Ed.), p. 247. Elsevier, Amsterdam/New York, 1982.
9. V. K. Tagirov, D. M. Chizhikov, E. K. Kazenas, and L. K. Shubochkin, *Inorg. Chem.* **20,** 1133 (1977).
10. Y. C. Long, Z. D. Zhang, K. Dwight, and A. Wold, *Mater. Res. Bull.* **23,** 631 (1988).
11. A. Hammou, E. Djurado, C. Roux, and C. Micheau, *in* "Proceedings of the 3rd International Symposium on Solid Oxide Fuel Cells" (S. C. Singhal and H. Iwahara, Eds.), Vol. 93(4), p. 48. The Electrochemical Society, Pennington, NJ, 1993.
12. E. Djurado, C. Roux, and A. Hammou, *J. Eur. Ceram. Soc.* **16,** 767 (1996).
13. M. T. Colomer and J. R. Jurado, *J. Non-Cryst. Solids* **217,** 48 (1997).
14. M. A. Spears, and H. L. Tuller, *in* "Proceedings of the Materials Research Society Symposium—Solid State Ionics III" (G. A. Nazri, J. M. Tascon, and M. Armand, Eds.), Vol. 293, p. 301. Materials Research Society, Pittsburgh, PA, 1993.
15. M. A. Spears and H. L. Tuller, *in* "Proceedings of the 2nd International Symposium on Ionic and Mixed Conducting Ceramics" (T. A. Ramanarayanan, W. L. Worrell, and H. L. Tuller, Eds.), Vol. 94(12), p. 94. The Electrochemical Society, Pennington, NJ, 1994.
16. B. Calès, and J.F. Baumard, *J. Electrochem. Soc.* **131,** 2407 (1984).
17. D. S. Patil, N. Venkataramani, and V. K. Rohatgi, *J. Mater. Sci.* **23,** 3367 (1988).
18. P. V. Ananthapadmanabhan, N. Venkatramani, V. K. Rohatgi, A. C. Momin, and K. S. Venkateswarlu, *J. Eur. Ceram. Soc.* **6,** 111 (1990).
19. S. S. Liou and W. L. Worrell, *Appl. Phys. A* **49,** 25 (1989).
20. S. S. Liou and W. L. Worrell, *in* "Proceedings of the 1st International Symposium on Solid Oxide Fuel Cells—Mixed-Conducting Oxide Electrodes for Solid Oxide Fuel Cells" (S. C. Singhal, Ed.), p. 81. The Electrochemical Society, Pennington, NJ, 1989.
21. R. M. C. Marques, J. R. Frade, and F. M. B. Marques, *in* "Proceedings Euroceramics II" (G. Ziegler and H. Hausner, Eds.), Vol. 3, p. 2179. Deutsche Keramische Gesellschaft, Augsburg, 1991.
22. H. Arashi and H. Naito, *Solid State Ionics* **53/56,** 431 (1992).
23. H. Naito and H. Arashi, *Solid State Ionics* **53/56,** 436 (1992).

24. R. M. C. Marques, J. R. Frade, and F. M. B. Marques, *in* "Proceedings of the 3rd International Symposium on Solid Oxide Fuel Cells" (S. C. Singhal and H. Iwahara, Eds.), Vol. 93(4), p. 513. The Electrochemical Society, Pennington, NJ, 1993.
25. M. T. Colomer, J. R. Jurado, R. M. C. Marques, and F. M. B. Marques, *in* "Proceedings of the 3rd International Symposium on Solid Oxide Fuel Cells" (S. C. Singhal, and H. Iwahara, Eds.), Vol. 93(4), p. 523, The Electrochemical Society, Pennington, NJ, 1993.
26. M. T. Colomer, J. R. Jurado, R. M. C. Marques, and F. M. B. Marques, *in* "Proceedings, Euroceramics III," (P. Durán, and J. F. Fernández, Eds.), Vol. 2, p. 293. Faenza Editrice Ibérica, Madrid, 1993.
27. T. Lindegaard, C. Clausen, and M. Mogensen, *in* "Proceedings of the 14th Riso International Symposium on Materials Science" (F. W. Poulsen, J. J. Bentzen, T. Jacobsen, E. Skou, and M. J. L. Ostergard, Eds.), p. 311. Riso National Laboratory, Roskilde, 1993.
28. M. T. Colomer, J. R. Jurado, R. M. C. Marques, and F. M. B. Marques, *in*: "Proceedings of the 2nd International Symposium on Ionic and Mixed Conducting Ceramics" (T. A. Ramanarayanan, W. L. Worrell, and H. L. Tuller, Eds.), Vol. 94(12), p. 369. The Electrochemical Society, Pennington, NJ, 1994.
29. H. Naito, and H. Arashi, *Solid State Ionics* **67,** 197 (1994).
30. R. M. C. Marques, F. M. B. Marques, and J. R. Frade, *Solid State Ionics* **73,** 15 (1994).
31. R. M. C. Marques, F. M. B. Marques, and J. R. Frade, *Solid State Ionics* **73,** 27 (1994).
32. M. T. Colomer, L. S. M. Traqueia, J. R. Jurado, and F. M. B. Marques, *Mater. Res. Bull.* **30,** 515 (1995).
33. R. M. C. Marques, F. M. B. Marques, and J. R. Frade, *in* "Ceramics—Charting the Future, Proceedings of the 8th CIMTEC–World Ceramics Congress, Part D" (P. Vicenzini, Ed.), p. 2625. Techna SRL, Faenza, 1995.
34. M. T. Colomer, Ph.D. Thesis, Universidad Autónoma, Madrid, 1995.
35. G. Róg and G. Borchardt, *Ceram. Int.* **22,** 149 (1996).
36. K. E. Swider, and W. L. Worrell, *J. Electrochem. Soc.* **143,** 3706 (1996).
37. M. T. Colomer, P. Durán, A. Caballero, and J. R. Jurado, *Mater. Sci. and Eng.* **A229,** 114 (1997).
38. J. Zarzycki, M. Prassas, and J. Phalippou, *J. Mater. Sci.* **17,** 3371 (1982).
39. F. M. B. Marques and G. P. Wirtz, *J. Am. Ceram. Soc.* **75,** 369 (1992).
40. G. P. Wirtz and F. M. B. Marques, *J. Am. Ceram. Soc.* **75,** 375 (1992).
41. G. Monrós, J. Carda, M. A. Tena, P. Escribano, M. Sales, and J. Alarcón, *J. Non-Cryst. Solids* **147/148,** 588 (1992).
42. K. E. Swider and W. L. Worrell, *J. Am. Ceram. Soc.* **78,** 961 (1995).
43. A. S. Sass, V. A. Shvets, G. A. Spieranskaya, G. A. Savielieva, and V. B. Kazansky, *Kinet. Katal.* **16,** 241 (1984).
44. R. D. Shannon and C. T. Prewitt, *Acta Crystallogr. B* **25**, 925 (1969).
45. L. S. M. Traqueia, T. Pagnier, and F. M. B. Marques, *J. Eur. Ceram. Soc.* **17,** 1019 (1997).
46. F. A. Kroger, and H. J. Vink, *Solid State Phys.* **3,** 307 (1956).